Cholesterol-mediated activation of acid sphingomyelinase disrupts autophagy in the retinal pigment epithelium

Kimberly A. Toops[a,b], Li Xuan Tan[a,c], Zhichun Jiang[d], Roxana A. Radu[d], and Aparna Lakkaraju[a,b,c]
[a]Department of Ophthalmology and Visual Sciences, School of Medicine and Public Health, [b]McPherson Eye Research Institute, and [c]Division of Pharmaceutical Sciences, School of Pharmacy, University of Wisconsin–Madison, Madison, WI 53706; [d]Jules Stein Eye Institute, University of California, Los Angeles, Los Angeles, CA 90024

ABSTRACT **Autophagy is an essential mechanism for clearing damaged organelles and proteins within the cell. As with neurodegenerative diseases, dysfunctional autophagy could contribute to blinding diseases such as macular degeneration. However, precisely how inefficient autophagy promotes retinal damage is unclear. In this study, we investigate innate mechanisms that modulate autophagy in the retinal pigment epithelium (RPE), a key site of insult in macular degeneration. High-speed live imaging of polarized adult primary RPE cells and data from a mouse model of early-onset macular degeneration identify a mechanism by which lipofuscin bisretinoids, visual cycle metabolites that progressively accumulate in the RPE, disrupt autophagy. We demonstrate that bisretinoids trap cholesterol and bis(monoacylglycero)phosphate, an acid sphingomyelinase (ASMase) cofactor, within the RPE. ASMase activation increases cellular ceramide, which promotes tubulin acetylation on stabilized microtubules. Live-imaging data show that autophagosome traffic and autophagic flux are inhibited in RPE with acetylated microtubules. Drugs that remove excess cholesterol or inhibit ASMase reverse this cascade of events and restore autophagosome motility and autophagic flux in the RPE. Because accumulation of lipofuscin bisretinoids and abnormal cholesterol homeostasis are implicated in macular degeneration, our studies suggest that ASMase could be a potential therapeutic target to ensure the efficient autophagy that maintains RPE health.**

Monitoring Editor
Jean E. Gruenberg
University of Geneva

Received: Jun 2, 2014
Revised: Oct 27, 2014
Accepted: Oct 27, 2014

INTRODUCTION

Macroautophagy (hereafter referred to as autophagy) is a bulk degradative pathway in which double-membraned structures called autophagosomes enclose damaged proteins and organelles. Fusion of autophagosomes with the endolysosomal system delivers hydrolytic enzymes required to degrade the sequestered cytosolic components (Rubinsztein *et al.*, 2007; Choi *et al.*, 2013). Formation of the autophagosome is initiated by the activation of autophagy-related (Atg) proteins in a hierarchical manner. The molecular machinery of autophagy is highly conserved and primarily regulated by the mammalian target of rapamycin (mTOR), in response to the nutrient and metabolic status of the cell. Autophagy occurs at a basal level in most cells and is increased under conditions of stress, when it promotes survival by repurposing degraded material to support metabolism within the cell (Codogno *et al.*, 2012).

Inefficient autophagy has been implicated in the pathogenesis of neurodegenerative diseases, because postmitotic neurons are especially susceptible to the accumulation of defective organelles and protein aggregates (Nixon, 2013). Autophagy is also critical for maintaining the health of the neural retina: in aged mice or mice with retina-specific deletions of *Atg5*, decreased autophagic flux precedes photoreceptor degeneration (Rodriguez-Muela *et al.*, 2013), and autophagy induction preserves differentiation of the

This article was published online ahead of print in MBoC in Press (http://www.molbiolcell.org/cgi/doi/10.1091/mbc.E14-05-1028) on November 5, 2014.

Address correspondence to: Aparna Lakkaraju (lakkaraju@wisc.edu).

Abbreviations used: ABCA4, ATP binding cassette transporter A4; AMD, age-related macular degeneration; ANOVA, analysis of variance; aPKC, atypical protein kinase C; ASMase, acid sphingomyelinase; Atg, autophagy-related; ATR, all-*trans*-retinal; BMP, bis(monoacylglycero)phosphate; BSA, bovine serum albumin; 11CR, 11-*cis*-retinal; FDA, U.S. Food and Drug Administration; HDAC6, histone deacetylase 6; JIP1, JNK-interacting protein 1; LXRα, liver X receptor alpha; mTOR, mammalian target of rapamycin; NPC1, Niemann-Pick C1; OS, outer segment; PBS, phosphate-buffered saline; RPE, retinal pigment epithelium; tfLC3, tandem fluorescent mRFP-GFP-LC3; TSA, trichostatin A; WIPI2, WD repeat domain, phosphoinositide interacting 2.

retinal pigment epithelium (RPE) and prevents photoreceptor death after oxidative stress (Zhao *et al.*, 2011) or exposure to Fas ligand (Besirli *et al.*, 2011). In the postmitotic RPE, which nourishes and supports the overlying photoreceptors, autophagy is increased in response to diverse stressors, including exposure to intense light, oxidative stress, mitochondrial poisons, cigarette smoke, and cell swelling (Reme *et al.*, 1999; Kunchithapautham and Rohrer, 2007a, b; Chen *et al.*, 2013; Doyle *et al.*, 2014; Wang *et al.*, 2014).

A key function performed by the RPE critical for photoreceptor health is the circadian phagocytosis and lysosomal degradation of shed photoreceptor outer segment (OS) tips (Bok, 1993). Each RPE cell contacts 30–50 photoreceptors, which shed ~10% of their OS length daily. Over a lifetime, this immense metabolic activity results in the progressive accumulation of undigested OS components called lipofuscin in RPE lysosomes (Sparrow *et al.*, 2012). RPE lipofuscin differs from that in other postmitotic tissues in that it is primarily composed of bisretinoid metabolites of vitamin A, generated as by-products of the visual cycle (Eldred and Lasky, 1993). Light induces isomerization of the visual chromophore 11-*cis*-retinal (11CR) to all-*trans*-retinal (ATR), which is flipped by the ATP binding cassette transporter A4 (ABCA4) from the lumen to the cytosolic side of the disk membrane and reduced to nontoxic all-*trans*-retinol by retinol dehydrogenase 8 (Weng *et al.*, 1999). Delayed removal of 11CR and ATR from disk membranes makes them susceptible to condensation reactions that ultimately result in the formation of vitamin A derivatives such as the lipofuscin bisretinoid A2E in RPE lysosomes (Sparrow *et al.*, 2012). Once formed, lipofuscin bisretinoids remain in the RPE for life, because their unique structures render them resistant to lysosomal degradation.

Chronic accumulation of these bisretinoids has been implicated in the pathology of numerous blinding retinal diseases, including Stargardt disease, Best disease, and age-related macular degeneration (AMD; Ambati and Fowler, 2012; Sparrow *et al.*, 2012). We previously demonstrated that A2E, a cone-shaped lipid, displaces cholesterol from lipid bilayers and sequesters cholesterol in RPE late endosomes and lysosomes (Lakkaraju *et al.*, 2007). Because membrane cholesterol levels modulate autophagosome–lysosome interactions (Fraldi *et al.*, 2010; Koga *et al.*, 2010; Sarkar *et al.*, 2013), we hypothesized that cholesterol storage induced by lipofuscin bisretinoids would inhibit autophagic clearance in the RPE. OS phagocytosis has been shown to recruit autophagic machinery in the RPE (Kim *et al.*, 2013; Frost *et al.*, 2014; Yao *et al.*, 2014), and inefficient autophagy is thought to play a part in the pathogenesis of retinal diseases such as AMD (Bowes Rickman *et al.*, 2013; Frost *et al.*, 2014). However, how innate processes such as progressive accumulation of lipofuscin bisretinoids impact autophagy in the RPE is not well understood.

In this paper, we report decreased autophagosome biogenesis and autophagic flux in the RPE of *ABCA4*$^{-/-}$ disease mice, which have high levels of A2E and other bisretinoids (Radu *et al.*, 2011). High-speed live imaging of primary RPE by spinning-disk confocal microscopy (Toops *et al.*, 2014) showed that A2E interfered with autophagosome biogenesis, constrained autophagosome traffic, and decreased autophagic flux. Our data unveil a stepwise molecular mechanism by which lipofuscin- and A2E-induced lysosomal cholesterol storage (Lakkaraju *et al.*, 2007) activates acid sphingomyelinase (ASMase) by sequestering the anionic lipid bis(monoacylglycero) phosphate (BMP), an ASMase cofactor (Kirkegaard *et al.*, 2010). The resulting increase in ceramide levels lead to increased tubulin acetylation (He *et al.*, 2012, 2014). Our data show that bidirectional motility of autophagosomes and autophagosome–lysosome fusion are impaired in cells with acetylated microtubules. In support of a central role for cholesterol-mediated ASMase activation in regulating autophagy, we demonstrate that a drug that promotes cholesterol efflux (Lakkaraju *et al.*, 2007) and a U.S. Food and Drug Administration (FDA)-approved ASMase inhibitor (Kornhuber *et al.*, 2010) restore efficient autophagosome transport and autophagic flux in the RPE.

There are two significant implications of our study: first, our data show that autophagy in the RPE is regulated in response to the immense metabolic demands placed on the cell, adding to a growing body of evidence for specialized regulation of autophagy based on tissue, function, and context (Grumati *et al.*, 2010; Jimenez-Sanchez *et al.*, 2012; Le Guezennec *et al.*, 2012; Pampliega *et al.*, 2013). Second, our studies suggest that ASMase inhibition could be a potential novel therapeutic strategy not only in macular degeneration associated with excess lipofuscin accumulation but also in diseases characterized by abnormal cholesterol homeostasis and impaired autophagy (Le Guezennec *et al.*, 2012; Nixon, 2013; Barmada *et al.*, 2014; Lee *et al.*, 2014).

RESULTS

Lipofuscin bisretinoids interfere with canonical autophagy in the RPE

To investigate whether lipofuscin bisretinoids impact autophagy in vivo, we measured microtubule-associated light chain 3B-II (LC3B-II) and p62/SQSTM1 levels in RPE of *ABCA4*$^{-/-}$ mice, which have high levels of lipofuscin bisretinoids such as A2E (Radu *et al.*, 2011). Conversion of LC3B-I to its lipidated form (LC3B-II) is an indicator of autophagosome biogenesis, and p62 levels are a measure of autophagic flux (Klionsky *et al.*, 2012). *ABCA4*$^{-/-}$ RPE had significantly less LC3B-II (Figure 1A) and more p62 (Figure 1B) compared with RPE from age-matched wild-type mice, supporting the hypothesis that accumulation of lipofuscin bisretinoids is associated with defective autophagy in vivo. To determine how lipofuscin bisretinoids inhibit autophagy in the RPE, we established an in vitro model by exposing polarized porcine primary RPE monolayers (Toops *et al.*, 2014) to the bisretinoid A2E, chronically (50 nM over 3 wk) or acutely (10 μM for 6 h), either of which result in intracellular A2E levels comparable with those seen in the RPE of *ABCA4*$^{-/-}$ mice and in human Stargardt disease patients (Supplemental Table S1).

In polarized primary RPE cells, autophagy was up-regulated after mTOR inhibition, either by nutrient deprivation or treatment with the selective mTOR inhibitors Torin 1 and Torin 2. We used tandem fluorescent monomeric red fluorescent protein (mRFP) enhanced green fluorescent protein (EGFP) LC3 (tfLC3) to monitor autophagy in primary RPE cells in real time. On fusion of autophagosomes with lysosomes, EGFP fluorescence is quenched in the acidic lysosomal pH, and only the pH-insensitive mRFP signal is visible; therefore ratios of EGFP to mRFP are a measure of autophagic flux (Klionsky *et al.*, 2012). TfLC3 imaging showed significantly more EGFP puncta in cells treated with A2E compared with control cells, both at the basal level and after mTOR inhibition either by nutrient deprivation or Torin treatment (Figure 1, C and D).

Immunoblotting of polarized primary RPE monolayers after mTOR inhibition showed significantly lower LC3B-II levels in cells treated with A2E compared with control RPE. The vacuolar ATPase inhibitor bafilomycin A1, which prevents lysosomal degradation of LC3B, increased LC3B-II after mTOR inhibition in control cells but not in cells exposed to A2E (Figure 1, E and F). To confirm that A2E decreased autophagosome biogenesis, we immunostained primary RPE monolayers for WD repeat domain, phosphoinositide interacting 2 (WIPI2)-positive preautophagosomal structures (Polson *et al.*, 2010). There were fewer WIPI2-labeled nascent autophagosomes at the basal state and after mTOR inhibition in cells with A2E, compared with

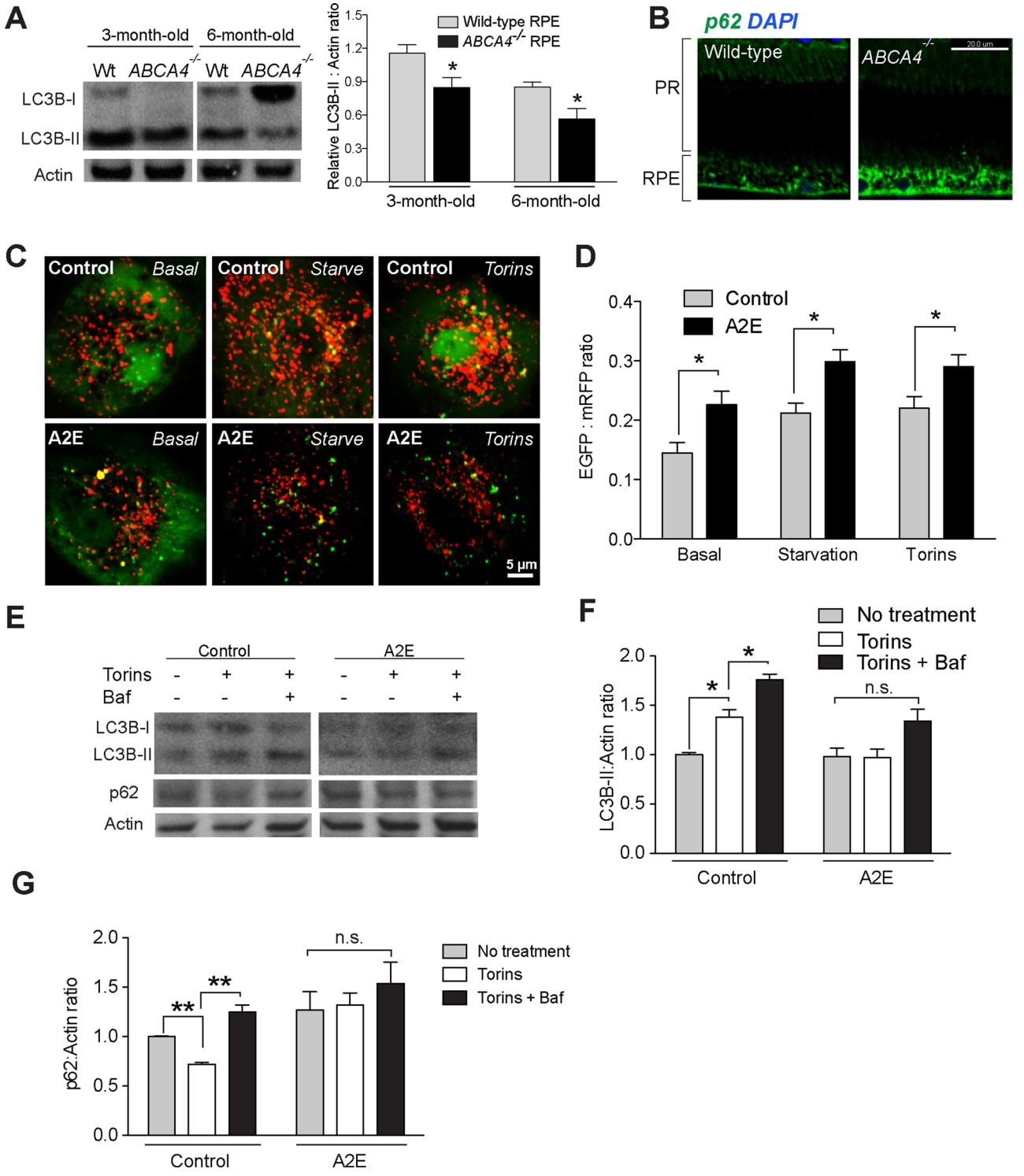

FIGURE 1: Regulation of autophagy in the RPE. (A) Representative immunoblot and quantification of LC3B-II levels in the RPE of 3- and 6-mo-old wild-type (gray bars) and *ABCA4*$^{-/-}$ (black bars) mice. Significantly less than age-matched wild-types, $n \geq 9$ animals per group; *, $p < 0.05$. (B) Immunohistochemistry for p62 (green) in retinal cryosections from 6-mo-old wild-type and *ABCA4*$^{-/-}$ mice. PR, photoreceptors; RPE, retinal pigment epithelium. Scale bar: 20 µm. (C) Stills from live imaging of tfLC3 in primary RPE to monitor basal autophagy and autophagic flux after mTOR inhibition by serum starvation or Torin1 and Torin 2 (both for 2 h). (D) Quantification of EGFP/mRFP ratios of cells in C. *, significantly greater than corresponding control cells, $p < 0.01$, $n = 30$ cells per condition. (E) Representative immunoblot of LC3B-I, LC3B-II, and p62 protein levels in control or A2E-laden primary RPE monolayers untreated or treated with torins ± bafilomycin A1 (Baf, 100 nM for 2 h). (F) Quantification of LC3B-II immunoblots, $n \geq 9$ per condition; *, $p < 0.01$; n.s., not significant. (G) Quantification of p62 immunoblots, $n \geq 9$ per condition; **, $p < 0.001$; n.s., not significant.

control cells (Supplemental Figure S1). Immunoblotting also showed that there was significantly more p62 in cells with A2E after Torin treatment (Figure 1, E and G), indicating a block in autophagic flux. Taken together, these data suggest that lipofuscin bisretinoids interfere with canonical autophagy in vivo in the *ABCA4*$^{-/-}$ mice and in primary RPE cells in culture.

Autophagosome trafficking is disrupted in RPE with the bisretinoid A2E

Because tfLC3 imaging and p62 immunoblotting data showed a block in autophagosome–lysosome fusion and decreased autophagic flux in RPE with bisretinoids, we asked whether A2E interfered with the trafficking of autophagosomes. We performed live imaging of EGFP-LC3–labeled autophagosomes in untreated or A2E-laden primary RPE cells using high-speed spinning-disk confocal microscopy. After serum starvation to induce autophagy, RPE with A2E had fewer EGFP-LC3 motile tracks compared with control cells (Figure 2, A and C, and Supplemental Movies S1 and S2). We used four-dimensional image analysis (Imaris, Bitplane) to quantify changes in autophagosome trajectories induced by A2E. To examine the efficiency of autophagosome transport, we used Spots and Tracks algorithms in Imaris to calculate how far each autophagosome traveled (track displacement length) as a function of the movement required to travel that distance (total track length) (Liu *et al.*, 2010). Analysis of track displacement data by Boolean gating showed a significant decrease in the population of autophagosomes with long-range, directed movements (large displacement with long track lengths) in cells with A2E (Figure 2, B and D, and Table 1). Compared with control cells, RPE with A2E had fewer motile autophagosomes (aggregate number of motile tracks was 17,010 in control cells and 5914 in cells with A2E), which moved with significantly lower velocities (Figure 2E). How could A2E, which is present in RPE late endosomes and lysosomes (Lakkaraju *et al.*, 2007), interfere with autophagosome trafficking?

Excess cholesterol mediates autophagic defects in RPE with bisretinoids

A critical determinant of organelle motility and fusion is membrane cholesterol (Lebrand *et al.*, 2002; Fraldi *et al.*, 2010). We showed previously that A2E, a cone-shaped lipid, competes with cholesterol (another cone-shaped lipid) for space under the phospholipid umbrella to minimize unfavorable interactions with the aqueous phase. Displacement of cholesterol from the lipid bilayer traps cholesterol within RPE late endosomes and lysosomes (Lakkaraju *et al.*, 2007). A2E and other lipofuscin bisretinoids increased total cell cholesterol measured biochemically in primary RPE after chronic or acute exposure (Figure 3A) and in the RPE of 3- and 6-mo-old *ABCA4*$^{-/-}$ mice (Figure 3B). We then asked whether A2E-induced cholesterol accumulation was responsible for autophagic defects. To test this, we treated cells with the liver X receptor alpha (LXRα) agonist TO901317, which transcriptionally activates ABCA1 and ABCG1 cholesterol transporters, to clear excess cholesterol in cells with A2E (Lakkaraju *et al.*, 2007; Supplemental Figure S2A). Immunoblotting and quantification of LC3B-II and p62 protein levels after mTOR inhibition showed that TO901317 increased autophagosome biogenesis (Figure 3, C and D) and autophagic flux in A2E-laden cells (Figure 3, C and E). We used live imaging of tfLC3 to follow autophagosome–lysosome fusion: TO901317 restored autophagic flux in cells with A2E and decreased EGFP fluorescence back to control levels (Figure 3, F and G). Collectively these data confirm that excess cholesterol induces defects in autophagosome trafficking and autophagosome–lysosome fusion in cells with lipofuscin bisretinoids.

Tubulin acetylation on stable microtubules impairs autophagosome trafficking

Intracellular trafficking is coordinated by the actin and microtubule cytoskeletons and associated motor proteins (Rodriguez-Boulan *et al.*, 2005). Organelle-specific recruitment of microtubule motors is accomplished in part by posttranslational modifications of α-tubulin such as acetylation and detyrosination, which preferentially occur on stable microtubules and cause cell type–specific alterations of organelle motility (Joseph *et al.*, 2008; Perdiz *et al.*, 2011). To examine how bisretinoid-induced cholesterol accumulation interferes with autophagy in the RPE, we asked whether altered microtubule stability and/or posttranslational tubulin modifications could explain the constrained trafficking of autophagosomes. Immunostaining showed that acetylated tubulin, which is mainly found in primary cilia of control RPE, increased dramatically in cells with A2E, with a corresponding decrease in tyrosinated tubulin (Figure 4, A and B). Neither total β-tubulin expression (Supplemental Figure S2B) nor the organization of the actin cytoskeleton (Supplemental Figure S2C) were altered in these cells. RPE from 6-mo-old *ABCA4*$^{-/-}$ mice had more acetylated tubulin compared with age-matched wild-types (Figure 4C), confirming that bisretinoids increase tubulin acetylation in vivo. Under conditions that depolymerize microtubules in polarized epithelia (nocodazole and cold treatment; Kreitzer *et al.*, 2003), there were significantly more acetylated microtubules in A2E-laden cells compared with controls (Figure 4, D and E), indicative of increased microtubule stability. Acetylated tubulin also increased in cells treated with U18666A, a drug that induces lysosomal cholesterol storage (Ko *et al.*, 2001; Supplemental Figure S2D), suggesting that cholesterol mediates the effects of A2E on microtubule stability and tubulin acetylation. To establish that hyperacetylation of tubulin disrupts autophagosome traffic, we performed live imaging of EGFP-LC3 trafficking in RPE treated with trichostatin A (TSA), an inhibitor of histone deacetylase 6 (HDAC6), the enzyme that deacetylates tubulin (Joseph *et al.*, 2008). Confirming our hypothesis, TSA treatment replicated the autophagosome trafficking defects seen in cells with A2E (Figure 4, F and G, Supplemental Movie S3, and Table 1). Thus bisretinoid-induced cholesterol storage prevents autophagosome trafficking by increasing tubulin acetylation.

ASMase activation promotes hyperacetylation of tubulin in the RPE

To dissect the molecular mechanism that links bisretinoid-stimulated cholesterol accumulation in the endolysosomal system with tubulin acetylation, we sought clues from cholesterol-storage disorders like Niemann-Pick C1 (NPC1). In NPC1 fibroblasts, excess cholesterol in late endosomes and lysosomes sequesters the anionic phospholipid BMP (Pipalia *et al.*, 2007). BMP is a cofactor for ASMase, the lysosomal enzyme that hydrolyzes sphingomyelin to generate ceramide (Kirkegaard *et al.*, 2010). Recent studies show that ceramide regulates tubulin acetylation via atypical protein kinase C (aPKC) and aurora A kinase (He *et al.*, 2012, 2014). In polarized primary RPE with A2E, immunofluorescence imaging showed high levels of BMP, which colocalized with filipin staining for cholesterol (Figure 5A). Cells with A2E also had high ASMase activity (Figure 5B) and more ceramide (Figure 5C) compared with control RPE. Treatment with desipramine, a functional inhibitor of ASMase (Kornhuber *et al.*, 2010), decreased ASMase activity and ceramide levels (Figure 5, B and C). Desipramine also decreased acetylated tubulin in cells with A2E (Figure 5D), confirming that cholesterol increases tubulin acetylation via a BMP-ASMase-ceramide pathway.

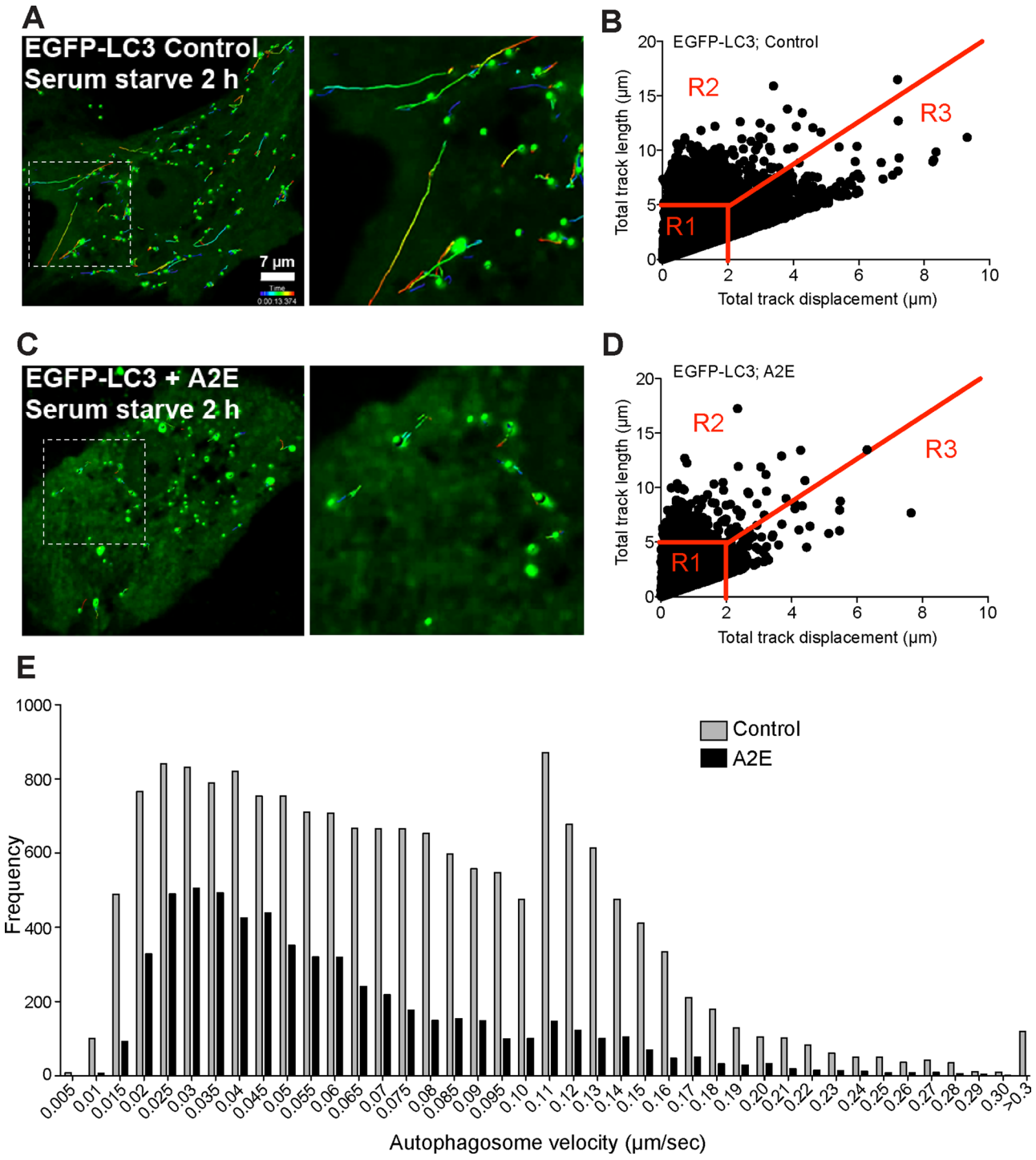

FIGURE 2: Live imaging of autophagosome trafficking in the RPE. (A and C) Stills from live imaging of EGFP-LC3 with spots and tracks superimposed in serum-starved RPE (A) untreated (control) or (C) exposed to A2E. Right, high-magnification images of areas denoted by white boxes on the left. (B and D) Plots of track displacement of EGFP-LC3–labeled autophagosomes vs. total track length in untreated cells (B) or cells exposed to A2E (D). Boolean gating was used to analyze data as explained in *Material and Methods*. See Table 1 for R1, R2, and R3 percentages. (E) Frequency histogram of EGFP-LC3–labeled autophagosome velocities (µm/sec) from Supplemental Movies S1 and S2. Gray bars, control cells; black bars, cells treated with A2E.

Inhibition of ASMase activity corrects autophagic defects in the RPE

If, as the above data indicate, ASMase is a critical regulator of autophagy, then ASMase inhibition should be sufficient to restore autophagic flux in RPE with bisretinoid-mediated cholesterol accumulation. We first performed live imaging of EFGP-LC3, and image analyses of trafficking data (Figure 6A and Supplemental Movies S4 and S5) showed that desipramine increased both the number of motile tracks and long-range displacement of autophagosomes in RPE cells with A2E (Figure 6, B–E, and Table 2). After mTOR

	Region 1 (R1) (D < 2 μm, L < 5 μm)	Region 2 (R2) (L > 5 μm, slope < 0.5 μm)	Region 3 (R3) (L > 5 μm, slope > 0.5 μm)
Control (%)	87.57	6.56	5.87
A2E (%)*	93.51	5.37	1.12
TSA (%)*	88.01	10.35	1.64

*Significantly different from control cells, $p < 0.0001$, one-way ANOVA.

TABLE 1: Quantitation of EGFP-LC3 trafficking data (from Figures 2 and 4).

inhibition, a short exposure to desipramine increased LC3B-II levels in RPE with A2E comparable with those in control cells (Figure 7, A and B). Desipramine also decreased p62 levels in cells with A2E (Figure 7, A and C), indicating a restoration of autophagic flux. In agreement with immunoblotting data, tfLC3 imaging showed that desipramine corrected defects in autophagosome–lysosome fusion after serum starvation (Figure 7D) and Torin treatment (Figure 7E) in RPE cells with A2E. Thus ASMase inhibition could be an effective therapeutic target to increase cellular clearance in RPE with lipofuscin bisretinoids.

DISCUSSION

We describe here a novel molecular mechanism by which autophagy is derailed by lipofuscin bisretinoids and excess cholesterol (Figure 8), which progressively accumulate in the RPE and contribute to the pathogenesis of macular degeneration (Ambati *et al.*, 2013; Bowes Rickman *et al.*, 2013; Pikuleva and Curcio, 2014). Although decreased autophagy within the retina is thought to participate in the pathogenesis of retinal dystrophies (Bowes Rickman *et al.*, 2013; Frost *et al.*, 2014), little is currently known about the precise mechanisms involved or how autophagy can be exploited as a potential drug target to maintain RPE health.

The data presented in this study identify ASMase as a critical regulator of autophagy in RPE compromised by lipofuscin-mediated cholesterol accumulation. We show that in cells with bisretinoids, cholesterol sequesters the anionic lipid BMP within RPE late endosomes and lysosomes. BMP activates ASMase, the enzyme that hydrolyzes sphingomyelin to ceramide, which in turn promotes tubulin acetylation on stable microtubules. Studies in polarized epithelia and neural progenitors show that ceramide inhibits the microtubule deacetylase HDAC6 by preventing the translocation of aPKC from the membrane to the cytosol. This interferes with aPKC-mediated phosphorylation of two HDAC6 activators, aurora A kinase and glycogen synthase kinase 3β, resulting in the accumulation of acetylated tubulin (He *et al.*, 2012, 2014). Ceramide can also phosphorylate the focal adhesion scaffold protein paxillin (Sasaki *et al.*, 1996), which has been recently identified as a negative regulator of HDAC6 activity (Deakin and Turner, 2014). Whether any of these mechanisms are responsible for ceramide-induced tubulin acetylation in RPE with bisretinoids remains to be determined.

Live-imaging data showed impaired autophagosome biogenesis and trafficking as a consequence of increased tubulin acetylation, either due to lipofuscin bisretinoids or after treatment with the HDAC6 inhibitor TSA. Acetylation is a posttranslational modification of α-tubulin that can act either singly or in concert with other modifications such as tyrosination/detyrosination to control motor recruitment in cargo-specific manner (Hammond *et al.*, 2008; Mackeh *et al.*, 2013). Precisely how posttranslational modifications of tubulin modulate the trafficking of autophagosomes and other organelles is not well understood. Acetylated microtubules in neurons preferentially recruit kinesin-1 and the scaffolding protein JNK-interacting protein 1 (JIP1) to direct polarized traffic to a subset of neurites (Reed *et al.*, 2006). Binding of JIP1 to the kinesin heavy-chain motor domain of kinesin-1 accelerates anterograde traffic, whereas JIP1 binding to the $p150^{Glued}$ subunit of the dynein–dynactin complex promotes retrograde traffic. JIP1 has recently been shown to bind LC3 in neurons to direct dynein-mediated retrograde transport of autophagosomes. Interestingly, the LC3-JIP1 interaction interferes with JIP1-mediated activation of kinesin-1 (Fu *et al.*, 2014). Unlike autophagosomes in neurons, which undergo unidirectional retrograde transport along the axon (Fu *et al.*, 2014), autophagosomes in the RPE, as shown by our data, exhibit bidirectional motility, likely driven by opposing actions of kinesin and dynein motors (Fu and Holzbaur, 2014). It is possible that acetylated microtubules in RPE with bisretinoids preferentially recruit kinesin-1 (Reed *et al.*, 2006), which would then compete with LC3 for JIP1 binding (Fu *et al.*, 2014). We also observed fewer tyrosinated microtubules in cells with A2E, which could interfere with the recruitment of $p150^{Glued}$/dynactin (Rocha *et al.*, 2009). Thus, in RPE with bisretinoids, increased acetylation and decreased tyrosination of tubulin could interfere with bidirectional autophagosome transport, possibly by altering the recruitment of motor proteins and/or preventing interactions between motors, scaffolds, and cargo. Further studies will help dissect the roles of these motor and scaffolding proteins in directing the transport of autophagosomes and other organelles (endosomes, lysosomes, phagosomes, etc.) in the RPE.

How might increased tubulin acetylation interfere with autophagosome biogenesis? At the earliest stages of autophagosome formation, phosphatidylinositol 3-phosphate binds its effectors WIPI1 and WIPI2 to catalyze the sequential recruitment of Atg proteins that regulate elongation of the preautophagosomal membrane. The fully formed Atg5-Atg12-Atg16L complex induces covalent conjugation of phosphatidylethanolamine to LC3 and facilitates autophagosome closure. Movement of these preautophagosomes along dynamic microtubules is necessary for both Atg recruitment and for driving subsequent steps of autophagosome formation (Geeraert *et al.*, 2010). It is therefore likely that increased stability of acetylated microtubules in cells with A2E interferes with the recruitment of Atg proteins, which decreases membrane elongation and autophagosome biogenesis.

Our data demonstrate that desipramine, a tricyclic antidepressant that increases ASMase proteolysis (Kornhuber *et al.*, 2010), restores autophagy in RPE with A2E by reversing ceramide-induced tubulin acetylation. Thus functional ASMase inhibitors, many of which are FDA-approved drugs with established safety and efficacy profiles (Kornhuber *et al.*, 2010), are promising candidates for inherited macular dystrophies characterized by elevated levels of lipofuscin bisretinoids such as Stargardt and Best diseases (Travis *et al.*, 2007). Lipofuscin bisretinoids are also implicated in AMD, the most common cause of vision loss in older adults (Ambati *et al.*, 2013). In this context, it is intriguing to note that allelic variants in cholesterol transporters and lipoprotein-metabolizing enzymes modulate susceptibility to AMD (Fritsche *et al.*, 2014) and that use of tricyclic antidepressants like desipramine is associated with a statistically significant decrease in the risk of developing early AMD (van Leeuwen *et al.*, 2004). Furthermore, ASMase activity and ceramide levels are increased in the brains of patients with Alzheimer's and Parkinson's diseases (Haughey *et al.*, 2010; Fabelo *et al.*, 2011), which are associated with dysregulated autophagy (Nixon, 2013). It is tempting to speculate that ASMase inhibition could be a novel therapeutic approach not only for retinal degeneration but also for neurodegenerative diseases.

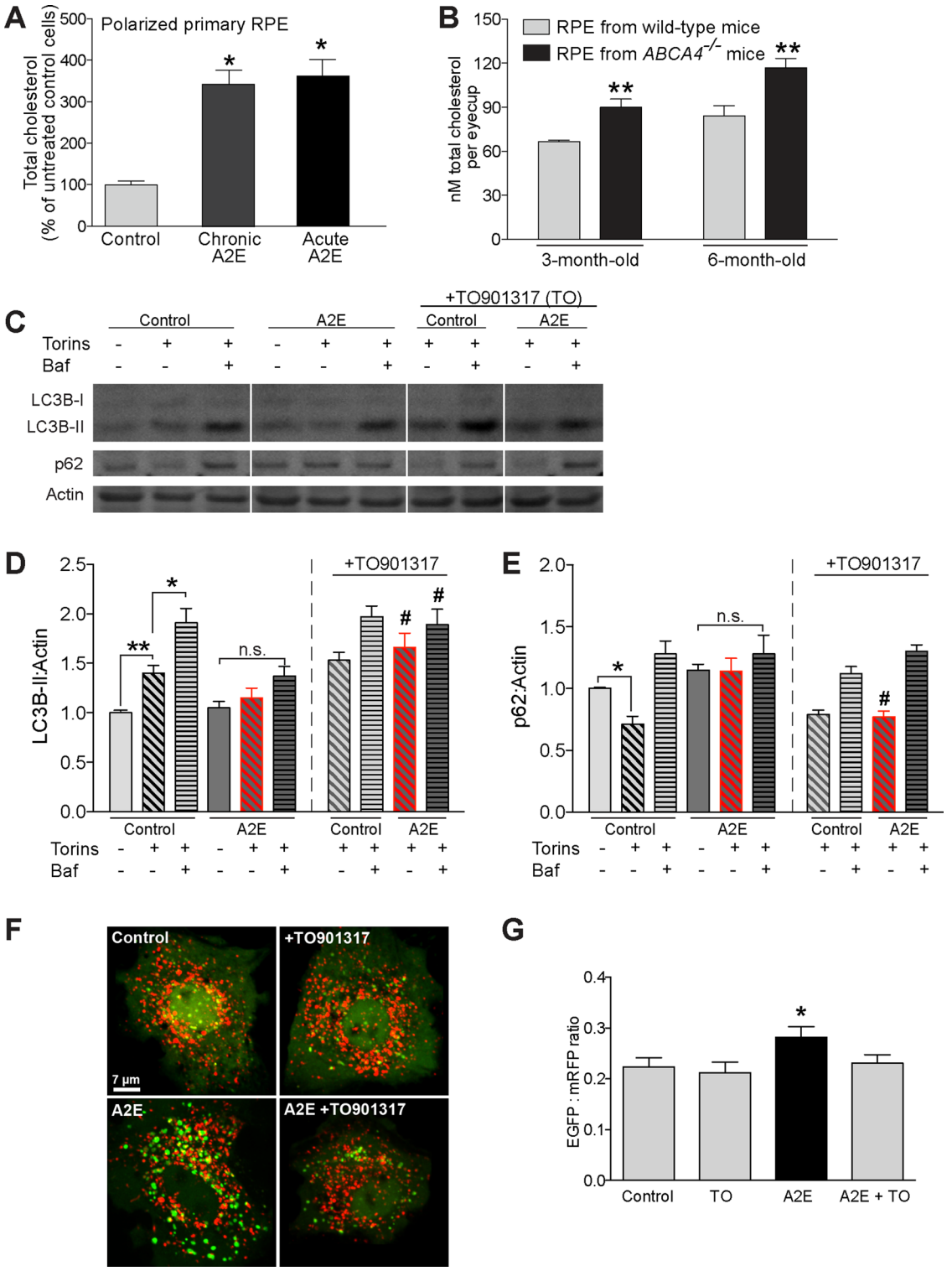

FIGURE 3: Cholesterol removal restores autophagosome biogenesis and autophagic flux in RPE with lipofuscin bisretinoids. (A) Biochemical quantification of cholesterol in polarized primary RPE, untreated (control) or exposed to A2E as indicated. Mean ± SEM, *, $p < 0.005$ relative to controls. (B) Total RPE cholesterol in eyecups from wild-type and *ABCA4*$^{-/-}$ mice. Mean ± SEM, $n \geq 9$ per group. **, $p < 0.005$ relative to age-matched wild-types. (C) Representative immunoblot of LC3B-I, LC3B-II, and p62 protein levels in control or A2E-laden primary RPE monolayers. Cells were untreated or treated with torins, bafilomycin (Baf, 100 nM for 2 h), and/or the LXRα agonist TO901317 (1 μM, 20 h), as indicated. (D) Quantification of LC3B-II immunoblots, $n \geq 9$ per condition; *, $p < 0.05$; **, $p < 0.01$; n.s., not significant; #, significantly greater than corresponding condition without TO901317 (in red hatched bars), $p < 0.05$. (E) Quantification of p62 immunoblots, $n \geq 9$ per condition; *, $p < 0.05$; n.s., not significant; #, significantly less than corresponding condition without TO901317 (in red hatched bars), $p < 0.05$. (F) Stills from live imaging of mRFP-GFP-LC3 in serum-starved RPE treated as indicated. (G) Quantification of EGFP (green) to mRFP (red) fluorescence in F. Mean ± SEM, *, significantly greater than all other treatments, $p < 0.05$.

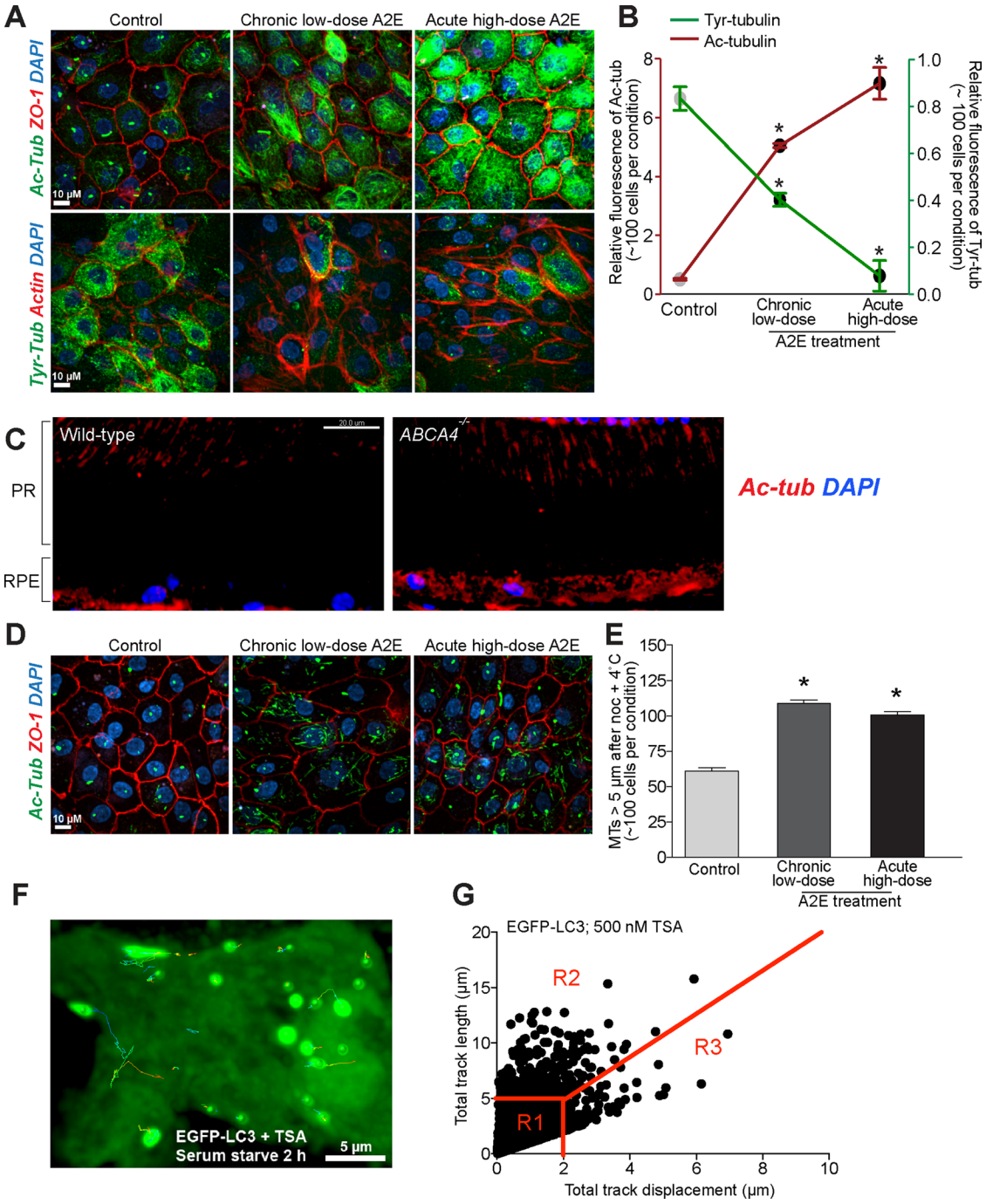

FIGURE 4: Tubulin acetylation modulates autophagosome trafficking in the RPE. (A) Immunofluorescence images of polarized primary RPE, untreated or exposed to A2E and stained for acetylated tubulin (green) and ZO-1 (red) or tyrosinated tubulin (green) and phalloidin to label actin (red). (B) Relative intensities of acetylated and tyrosinated tubulin staining in RPE. Mean ± SEM, *, $p < 0.0001$ relative to corresponding controls. (C) Immunohistochemistry for acetylated tubulin (red) in retinal cryosections from 6-mo-old wild-type and *ABCA4*$^{-/-}$ mice. PR, photoreceptors; RPE, retinal pigment epithelium. Scale bar: 20 μm. (D) Cells stained for acetylated tubulin (green) and ZO-1 (red) after nocodazole (33 μM) and cold treatment for 30 min. (E) Number of acetylated microtubules longer than 5 μm after nocodazole and cold treatment. Mean ± SEM, *, $p < 0.0001$. (F) Still from live imaging of EGFP-LC3 trafficking with spots and tracks superimposed in primary RPE treated with the HDAC6 inhibitor TSA (500 nM). (G) Track displacement of EGFP-LC3–labeled autophagosomes vs. total track length in TSA-treated cells in F analyzed by Boolean gating (see Table 1 for values).

MATERIALS AND METHODS

Cells

Primary RPE were harvested from freshly enucleated porcine eyes (Hart and Vold, Baraboo, WI) as previously described (Toops *et al.*, 2014): briefly, the anterior segment was removed at the ora serrata, and the retina was gently detached by clipping at the optic nerve head. RPE cells were isolated from eyecups upon incubation with 0.5% trypsin with 5.3 mM EDTA in Hank's balanced salt

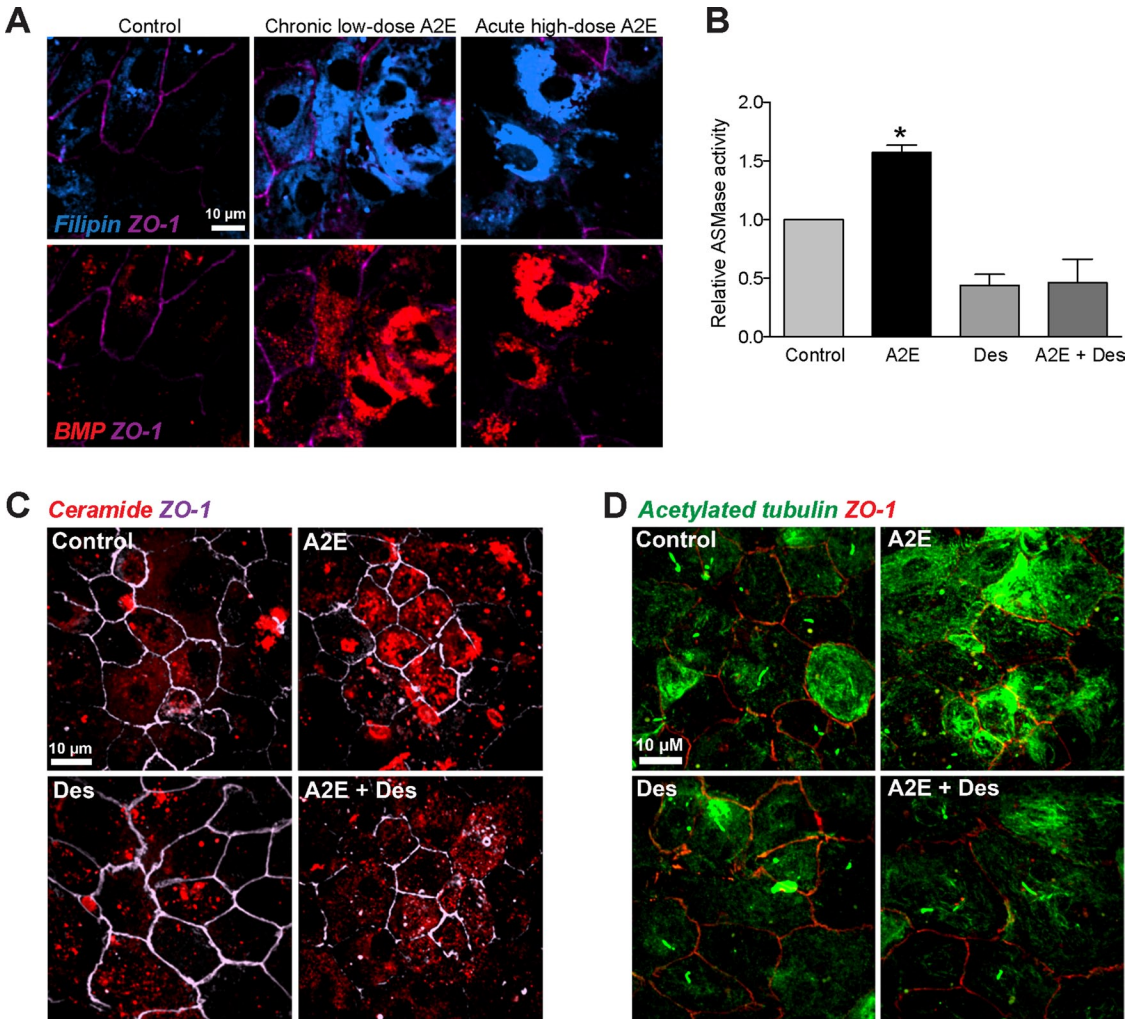

FIGURE 5: BMP-mediated activation of ASMase promotes tubulin acetylation. (A) Immunofluorescence images of polarized primary RPE, untreated (Control) or exposed to A2E, as indicated, labeled with filipin (blue) and stained for BMP (red) and ZO-1 (purple). (B) ASMase activity in primary RPE untreated (control) or treated with A2E and/or the ASMase inhibitor desipramine (Des, 10 μM for 3 h). *, $p < 0.005$ relative to all other conditions (one-way ANOVA, Dunnett's posttest). (C) Immunofluorescence staining for ceramide (red) and ZO-1 (white) in untreated cells (control) or cells treated with A2E and/or desipramine. (D) Immunofluorescence staining for acetylated tubulin (green) and ZO-1 (red) in untreated cells (control) or cells treated with A2E and/or desipramine.

solution and plated onto T25 flasks in DMEM with 1% heat-inactivated fetal bovine serum (FBS; American Type Culture Collection, Manassas, VA). For generation of polarized cultures, cells were plated at confluence (~300,000 cells/cm^2) onto collagen-coated Transwell (Corning, Corning, NY) semipermeable membrane filters. After 2 wk, monolayers had transepithelial electrical resistances of >300 ohm.cm^2, localized Na^+, K^+-ATPase apically, and expressed tight junction proteins (e.g., ZO-1) and RPE differentiation markers (e.g., RPE65) (Toops *et al.*, 2014).

Animals

Wild-type and *ABCA4*$^{-/-}$ mice (both 129/Sv strain on Rpe65 Leu-450 background) were raised under a 12-h cyclical light and fed a standard rodent diet (NIH-31, 7013; Harlan Teklad, Madison, WI). Mouse studies were done in adherence to guidelines established by the University of California–Los Angeles Animal Research Committee and the Association for Research in Vision and Ophthalmology statement for the Use of Animals in Ophthalmic and Vision Research. Animals were killed ~4–6 h after light onset and eyes were removed and hemisected. The anterior portion containing the cornea, lens, and vitreous was discarded. Eyecups containing retina, RPE, choroid, and sclera were frozen in liquid N_2 and stored at –80°C for further processing (Radu *et al.*, 2011).

Immunoblotting

RPE harvested from mouse eyecups were sonicated in lysis buffer with protease inhibitors for 10 min. Primary RPE on Transwell filters were harvested and lysed with NE-PER nuclear and cytoplasmic extraction reagents (#78833; Thermo Scientific, Rockford, IL) according to the manufacturer's recommendation. Protein concentrations were measured with DC assay (Bio-Rad, Hercules, CA). Samples (20 μg/lane) were resolved in 4–12% NuPAGE Bis-Tris Precast Gels (Invitrogen, Carlsbad, CA) at 130 V. Proteins were then transferred onto nitrocellulose membrane using the iBlot dry transfer system (Invitrogen) and blocked in 5% milk in Tris buffered saline with Tween20 (TBS-T) for 1 h before being incubated in primary antibody overnight at 4°C. Membranes were probed with antibodies to LC3B (1:3000; Novus [St. Louis, MO] NB600-1384 for pig and 1:500; Sigma-Aldrich [St. Louis, MO] L7543 for mouse), p62/SQSTM1 (1:1000; American Research Products [Waltham, MA]

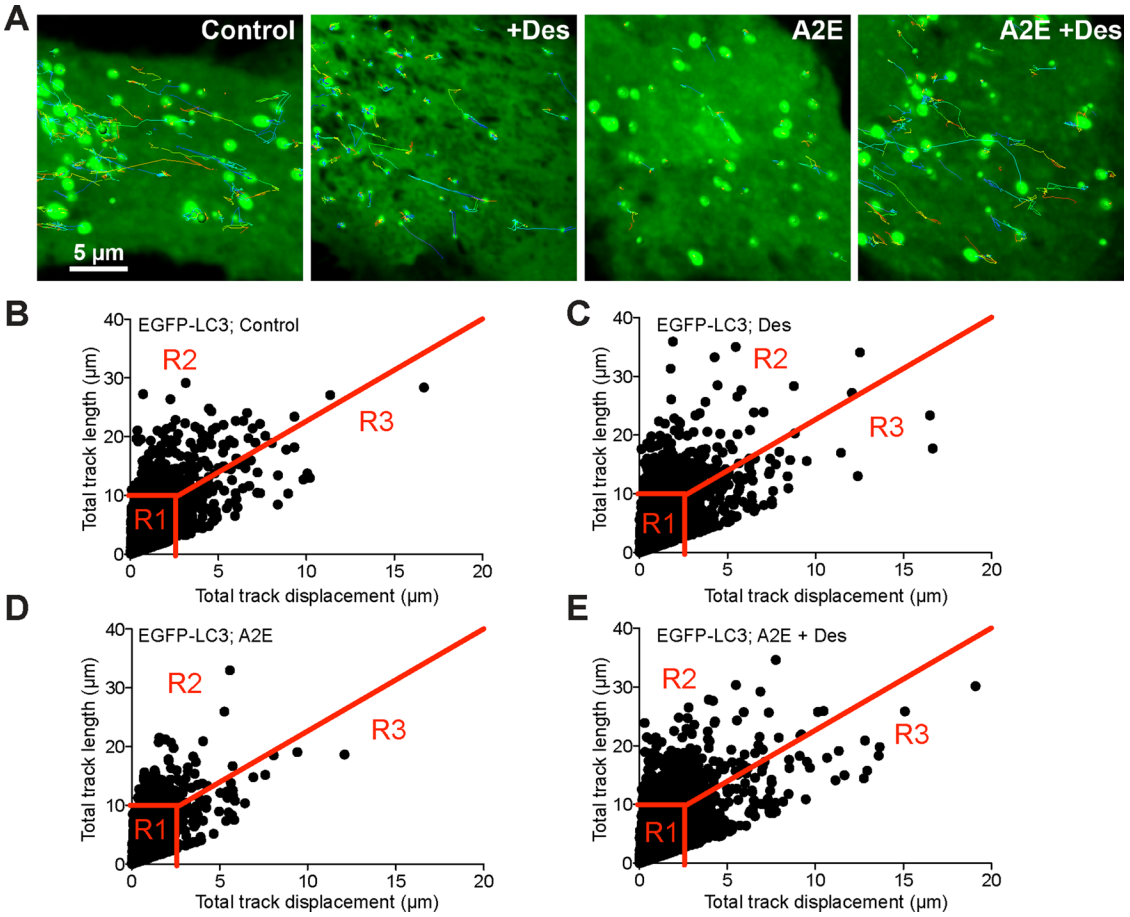

FIGURE 6: Desipramine corrects autophagosome trafficking defects in the RPE. (A) Stills from live imaging of EGFP-LC3 with spots and tracks superimposed in serum-starved RPE treated as indicated. Des, desipramine. (B–E) Analyses of live-imaging data depicted as track displacement of EGFP-LC3–labeled autophagosomes vs. total track length in control cells and cells treated with A2E and/or desipramine. Boolean gating was used to analyze data as explained in *Materials and Methods*. See Table 2 for R1, R2, and R3 percentages.

ARP03-GP62-C) and actin (1:5000; Santa Cruz Biotechnology, Dallas, TX) followed by horseradish peroxidase–conjugated secondary antibodies. Immunoblots were visualized by ECL substrate (Thermo Scientific) and quantified using Image Studio (LI-COR, Lincoln, NE).

Pharmacological treatments

The lipofuscin bisretinoid A2E was synthesized according to published protocols and purified by high-performance liquid chromatography (HPLC; >97%, electrospray ionization mass spectrometry; Lakkaraju *et al.*, 2007). RPE were exposed to either a chronic low-dose of A2E (50 nM for 3 wk) or an acute high-dose of A2E (10 µM for 6 h, followed by a 48-h chase). Quantification of A2E levels in cells was performed by HPLC as previously reported (Radu *et al.*, 2011). Other drugs used were the mTOR inhibitors Torin 1 and Torin 2 (50 nM and 1.5 µM, respectively, for 2 h; Tocris Bioscience, Bristol, UK), the vacuolar ATPase inhibitor bafilomycin A1 (100 nM for 2 h; EMD Millipore, Billerica, MA), the LXRα agonist TO901317 (1 µM for 20 h; Cayman Chemicals, Ann Arbor, MI), the HDAC6 inhibitor TSA (500 nM, 16 h; Sigma-Aldrich), and the ASMase inhibitor desipramine (10 µM for 3 h; Sigma-Aldrich). For depolymerization of MTs, cells were treated with 33 µM nocodazole for 30 min; this was followed by cold treatment (4°C) for 30 min (Kreitzer *et al.*, 2003). At the concentrations and exposure times used, none of these drugs caused alterations in RPE cell morphology or physiology (monitored by TER measurements and ZO-1 and organelle marker staining).

Immunofluorescence staining and quantification

Filter-grown cells were fixed in 2% paraformaldehyde for 10 min, blocked in 1% bovine serum albumin (BSA) in phosphate-buffered saline (PBS), and incubated with specific primary antibodies for 1 h: mouse monoclonal anti–acetylated tubulin clone 6-11B-1 (1:1000; Sigma-Aldrich), rat monoclonal anti-tyrosinated α-tubulin (1:200; Santa Cruz), mouse anti-LBPA (1:500; Echelon Biosciences, Salt Lake, UT; Z-LBPA), mouse anti-ceramide (1:10; Enzo Life Sciences, Farmingdale, NY) and rat anti–Z0-1 (1:3000; Xu *et al.*, 2012). Alexa Fluor secondary antibodies were used at 1:500 and rhodamine–phalloidin (Cytoskeleton, Denver, CO; PHDR1) at 1:200. Filters were mounted under coverslips on glass slides under Vectashield

	Region 1 (R1) (D < 2.5 µm, L < 10 µm)	Region 2 (R2) (L > 10 µm, slope < 0.5 µm)	Region 3 (R3) (L > 10 µm, slope > 0.5 µm)
Control (%)	85.73	7.57	6.7
Des (%)	84.28	7.79	7.93
A2E (%)*	91.43	5.28	3.29
A2E+des (%)	83.88	7.77	8.35

*Significantly different from all other conditions, $p < 0.0001$, one-way ANOVA.

TABLE 2: Quantitation of EGFP-LC3 trafficking data (from Figure 6, B–E).

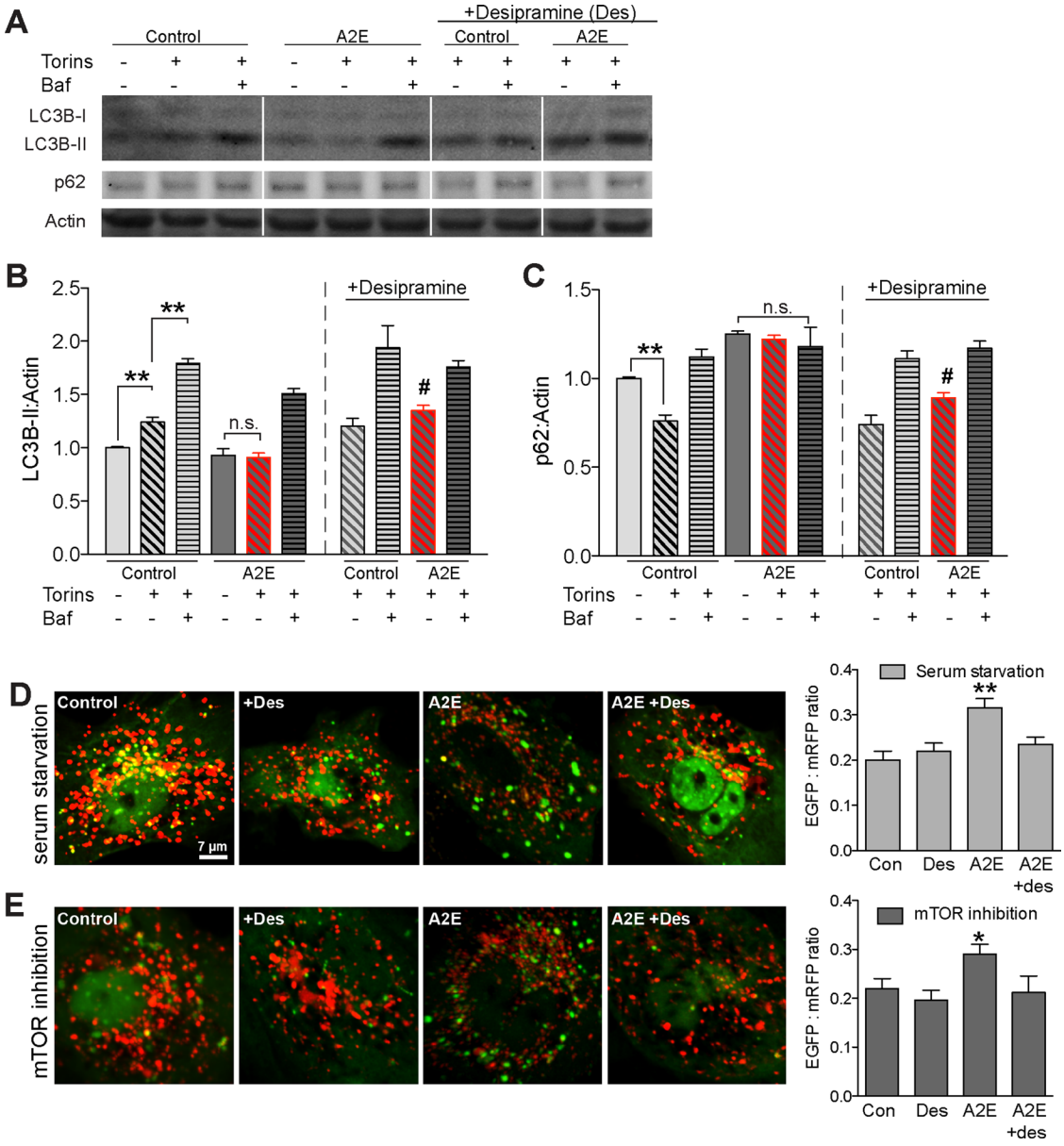

FIGURE 7: Inhibition of ASMase activity restores autophagic flux in RPE with the lipofuscin bisretinoid A2E. (A) Representative immunoblot of LC3B-I, LC3B-II, and p62 protein levels in control or A2E-laden primary RPE monolayers. Cells were untreated or treated with torins, bafilomycin (Baf, 100 nM for 2 h), and desipramine (Des, 10 µM, 3 h) as indicated. (B) Quantification of LC3B-II immunoblots, $n \geq 9$ per condition; **, p 0.01; n.s., not significant; #, significantly greater than corresponding condition without desipramine (in red hatched bars), $p < 0.01$. (C) Quantification of p62 immunoblots, $n \geq 9$ per condition; **, $p < 0.01$; n.s., not significant; #, significantly lesser than corresponding condition without desipramine (in red hatched bars), $p < 0.001$. (D) Stills from live imaging of mRFP-GFP-LC3 and quantification of EGFP/mRFP ratios in serum-starved RPE treated as indicated. **, significantly greater than all other treatments, $p < 0.0001$. (E) Stills from live imaging of tfLC3 and quantification of EGFP/mRFP ratios in torin-treated RPE treated as indicated. *, significantly greater than all other treatments, $p < 0.01$.

(Vector Labs, Peterborough, UK), sealed and visualized with an Andor (Belfast, UK) Revolution XD spinning-disk confocal microscope using a 60×/1.4 NA oil objective with identical exposures and gains for each antibody. Acetylated tubulin-labeled stable microtubules (≥5 µm in length) after nocodazole treatment were analyzed manually in the Surpass mode of Imaris (Bitplane, South Windsor, CT).

Immunohistochemistry

Cryosections of wild-type and *ABCA4*$^{-/-}$ mouse retinas were blocked in PBS with 4% BSA and incubated with primary antibodies (diluted 1:100 in PBS with 4% BSA) for 48 h at 4°C in a humidified chamber. Slides were rinsed to remove unbound antibodies and incubated with Alexa Fluor–conjugated secondary antibodies (1:500 in PBS with 4% BSA) for 18 h at 4°C in a humidified chamber protected from light. Sections were rinsed, stained with 4′,6-diamidino-2-phenylindole for 5 min, and rinsed and sealed under coverslips using Vectashield as a mounting medium. Slides were imaged with the Andor Revolution XD spinning-disk confocal microscope using a 40×/1.4 NA oil objective with identical exposures and gains for each antibody.

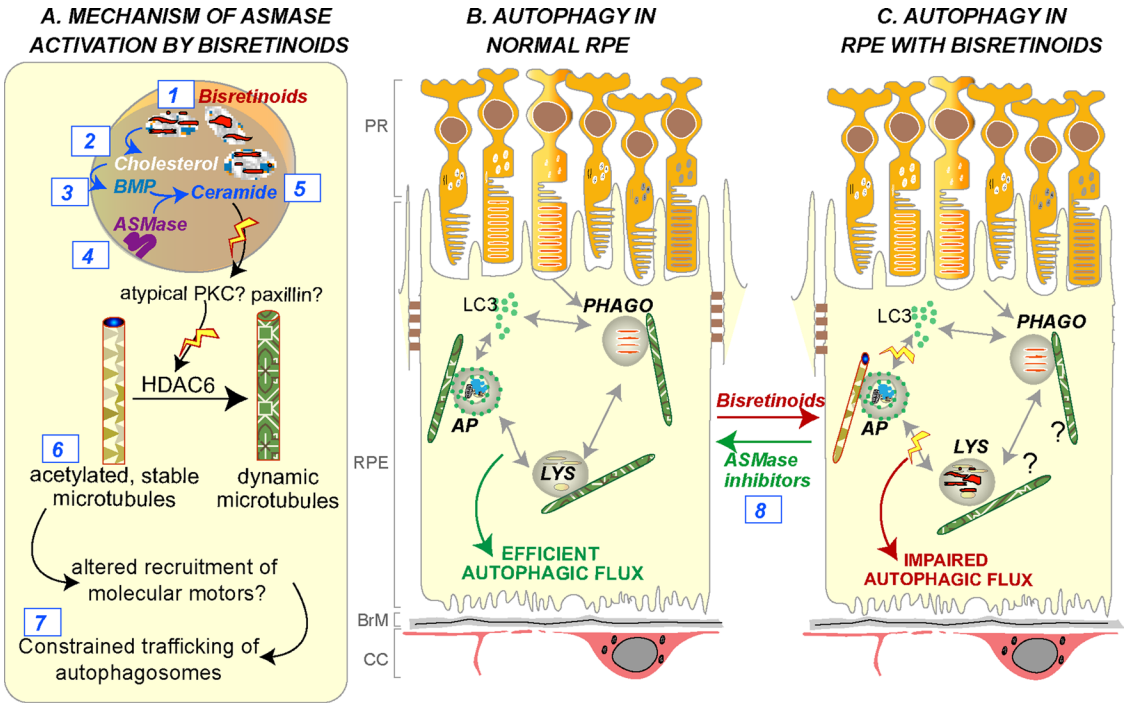

FIGURE 8: Model for impaired autophagy in RPE with bisretinoids. (A) Cone-shaped bisretinoids like A2E (1) sequester cholesterol (2) in RPE late endosomes and lysosomes, as we have reported previously (Lakkaraju *et al.*, 2007). Data presented in this study show that excess cholesterol in turn traps BMP (3), which activates ASMase (4), leading to increased production of ceramide from sphingomyelin (5). Ceramide promotes tubulin acetylation on stable microtubules (6), possibly by inhibiting HDAC6. Acetylated microtubules in the RPE interfere with autophagosome motility (7). (B) In normal RPE, autophagosome biogenesis and transport are essential for efficient autophagic flux. (C) Our data show that, in RPE with bisretinoids, aberrant activation of ASMase interferes with multiple steps of autophagy by increasing ceramide-induced tubulin acetylation. Whether acetylated microtubules also interfere with the trafficking of other organelles like phagosomes, endosomes, and lysosomes is currently under investigation. Drugs that inhibit ASMase decrease tubulin acetylation and increase autophagy in cells with lipofuscin bisretinoids (8).

Transfections

RPE cells were transfected with EGFP-LC3 (Addgene, Cambridge, MA; plasmid # 21073) or tfLC3 (Addgene; plasmid #21075) using the Amaxa nucleofector II (Lonza, Rockland, ME). Approximately 1.5 million cells and 5 µg plasmid DNA were used for each transfection. Cells were plated on either serum-coated glass-bottom dishes (MatTek, Ashland, MA) or Transwell filters at confluence.

Spinning-disk microscopy

Live imaging of autophagosome traffic and autophagic flux was performed on the Revolution XD spinning-disk microscopy system (Andor) equipped with the Yokogawa CSU-X1 confocal spinning-disk head; Nikon Eclipse Ti inverted microscope surrounded by an Okolab cage incubator; iXon x3 897 EM-CCD camera; Andor laser combiner with four solid-state lasers at 405, 488, 561, and 640 nm and corresponding band-pass filter sets (Sutter, Novato, CA); and ASI motorized stage with piezo-Z for rapid Z-stack acquisition. Andor IQ2 software was used for image acquisition and Imaris ×64 (Bitplane) for image analysis. For live imaging, cells were serum starved for 2 h to induce autophagy and rapid Z-stacks were acquired using the 100×/1.49 NA Apo TIRF objective (Nikon, Melville, NY) for ~50 frames at 37°C. Trafficking data were collected from three separate transfections for a total of at least 12–30 movies captured for treatment. During image acquisition, care was taken to maintain the same laser power, exposure and electron-multiplying gain settings. Trafficking analysis was carried out using the Spots and Tracks modules of the Imaris software (Liu *et al.*, 2010). After background subtraction (using the background-subtraction algorithm and identical automatic threshold for all images) and smoothing (Gaussian algorithm with identical threshold settings for all images), Spots and Tracks algorithms were used to identify vesicles and follow them through time and cell space to obtain total track length and track displacement. Statistical analysis of these data sets was performed using Excel (Microsoft, Redmond, WA) and Prism (GraphPad, La Jolla, CA).

Biochemical assays

Cells were harvested by trypsinization, and cell pellets were washed with PBS to remove residual medium. Cells were lysed in HNTG lysis buffer (50 mM HEPES, pH 7.4, 150 mM NaCl, 10% glycerol, 1.5 mM $MgCl_2$, 1% Triton X-100) supplemented with protease inhibitors. Total protein was measured using the DC protein assay kit (Bio-Rad). Cellular cholesterol was quantified using the Amplex Red cholesterol assay kit (Invitrogen) as detailed previously (Lakkaraju *et al.*, 2007). Single eyecups from wild-type and *ABCA4*$^{-/-}$ mice were homogenized in 50 µl of lysis buffer and processed as above. For measuring ASMase activity, cells were lysed in acidic pH, and assays were performed using the sphingomyelinase fluorometric assay kit from Cayman Chemicals according to the manufacturer's protocol.

Statistical analysis

Data were analyzed using either a two-tailed *t* test or one-way analysis of variance (ANOVA) followed by Bonferroni or Dunnett's post-tests (GraphPad Prism). Unless otherwise stated, data are presented as mean ± SEM of three or more independent experiments, with three to four replicates per condition per experiment. To analyze

EGFP-LC3 trafficking data, we used Boolean gating to segment three regions (denoted by R1, R2, and R3 on the track displacement vs. total track length graphs). Regions were defined by: minimum or maximum track length, minimum or maximum displacement, and a slope of 0.5 (displacement divided by length). Tracks with a slope <0.5 were taken as less straight (R2) than those with a slope of >0.5 (R3). Tracks within each region are represented as a percent of total number of tracks in Tables 1 and 2. One-way ANOVA or *t* tests were used to compare regions between treatment groups.

ACKNOWLEDGMENTS

This work was supported by National Institutes of Health grant P30 EY016665 and grants from Research to Prevent Blindness, American Federation for Aging Research, BrightFocus Foundation, Karl Kirchgessner Vision Research Foundation, and the Reeves Foundation for Macular Degeneration Research. A.L. is the Retina Research Foundation Rebecca Meyer Brown Professor and the recipient of a career development award from the Research to Prevent Blindness Foundation.

REFERENCES

Ambati J, Atkinson JP, Gelfand BD (2013). Immunology of age-related macular degeneration. Nat Rev Immunol 13, 438–451.

Ambati J, Fowler BJ (2012). Mechanisms of age-related macular degeneration. Neuron 75, 26–39.

Barmada SJ, Serio A, Arjun A, Bilican B, Daub A, Ando DM, Tsvetkov A, Pleiss M, Li X, Peisach D, *et al.* (2014). Autophagy induction enhances TDP43 turnover and survival in neuronal ALS models. Nat Chem Biol 10, 677–685.

Besirli CG, Chinskey ND, Zheng QD, Zacks DN (2011). Autophagy activation in the injured photoreceptor inhibits fas-mediated apoptosis. Invest Ophthalmol Vis Sci 52, 4193–4199.

Bok D (1993). The retinal pigment epithelium: a versatile partner in vision. J Cell Sci Suppl 17, 189–195.

Bowes Rickman C, Farsiu S, Toth CA, Klingeborn M (2013). Dry age-related macular degeneration: mechanisms, therapeutic targets, and imaging. Invest Ophthalmol Vis Sci 54, ORSF68–80.

Chen Y, Sawada O, Kohno H, Le YZ, Subauste C, Maeda T, Maeda A (2013). Autophagy protects the retina from light-induced degeneration. J Biol Chem 288, 7506–7518.

Choi AM, Ryter SW, Levine B (2013). Autophagy in human health and disease. N Engl J Med 368, 651–662.

Codogno P, Mehrpour M, Proikas-Cezanne T (2012). Canonical and non-canonical autophagy: variations on a common theme of self-eating? Nat Rev Mol Cell Biol 13, 7–12.

Deakin NO, Turner CE (2014). Paxillin inhibits HDAC6 to regulate microtubule acetylation, Golgi structure, and polarized migration. J Cell Biol 206, 395–413.

Doyle SL, Ozaki E, Brennan K, Humphries MM, Mulfaul K, Keaney J, Kenna PF, Maminishkis A, Kiang AS, Saunders SP, *et al.* (2014). IL-18 attenuates experimental choroidal neovascularization as a potential therapy for wet age-related macular degeneration. Sci Transl Med 6, 230ra244.

Eldred GE, Lasky MR (1993). Retinal age pigments generated by self-assembling lysosomotropic detergents. Nature 361, 724–726.

Fabelo N, Martin V, Santpere G, Marin R, Torrent L, Ferrer I, Diaz M (2011). Severe alterations in lipid composition of frontal cortex lipid rafts from Parkinson's disease and incidental Parkinson's disease. Mol Med 17, 1107–1118.

Fraldi A, Annunziata F, Lombardi A, Kaiser HJ, Medina DL, Spampanato C, Fedele AO, Polishchuk R, Sorrentino NC, Simons K, Ballabio A (2010). Lysosomal fusion and SNARE function are impaired by cholesterol accumulation in lysosomal storage disorders. EMBO J 29, 3607–3620.

Fritsche LG, Fariss RN, Stambolian D, Abecasis GR, Curcio CA, Swaroop A (2014). Age-related macular degeneration: genetics and biology coming together. Annu Rev Genomics Hum Genet 15, 151–171.

Frost LS, Mitchell CH, Boesze-Battaglia K (2014). Autophagy in the eye: implications for ocular cell health. Exp Eye Res 124, 56–66.

Fu MM, Holzbaur EL (2014). Integrated regulation of motor-driven organelle transport by scaffolding proteins. Trends Cell Biol 24, 564–574.

Fu MM, Nirschl JJ, Holzbaur EL (2014). LC3 binding to the scaffolding protein JIP1 regulates processive dynein-driven transport of autophagosomes. Dev Cell 29, 577–590.

Geeraert C, Ratier A, Pfisterer SG, Perdiz D, Cantaloube I, Rouault A, Pattingre S, Proikas-Cezanne T, Codogno P, Pous C (2010). Starvation-induced hyperacetylation of tubulin is required for the stimulation of autophagy by nutrient deprivation. J Biol Chem 285, 24184–24194.

Grumati P, Coletto L, Sabatelli P, Cescon M, Angelin A, Bertaggia E, Blaauw B, Urciuolo A, Tiepolo T, Merlini L, *et al.* (2010). Autophagy is defective in collagen VI muscular dystrophies, and its reactivation rescues myofiber degeneration. Nat Med 16, 1313–1320.

Hammond JW, Cai D, Verhey KJ (2008). Tubulin modifications and their cellular functions. Curr Opin Cell Biol 20, 71–76.

Haughey NJ, Bandaru VV, Bae M, Mattson MP (2010). Roles for dysfunctional sphingolipid metabolism in Alzheimer's disease neuropathogenesis. Biochim Biophys Acta 1801, 878–886.

He Q, Wang G, Dasgupta S, Dinkins M, Zhu G, Bieberich E (2012). Characterization of an apical ceramide-enriched compartment regulating ciliogenesis. Mol Biol Cell 23, 3156–3166.

He Q, Wang G, Wakade S, Dasgupta S, Dinkins M, Kong JN, Spassieva SD, Bieberich E (2014). Primary cilia in stem cells and neural progenitors are regulated by neutral sphingomyelinase 2 and ceramide. Mol Biol Cell 25, 1715–1729.

Jimenez-Sanchez M, Menzies FM, Chang YY, Simecek N, Neufeld TP, Rubinsztein DC (2012). The Hedgehog signalling pathway regulates autophagy. Nat Commun 3, 1200.

Joseph RA, Shepard BD, Kannarkat GT, Rutledge TM, Tuma DJ, Tuma PL (2008). Microtubule acetylation and stability may explain alcohol-induced alterations in hepatic protein trafficking. Hepatology 47, 1745–1753.

Kim JY, Zhao H, Martinez J, Doggett TA, Kolesnikov AV, Tang PH, Ablonczy Z, Chan CC, Zhou Z, Green DR, Ferguson TA (2013). Noncanonical autophagy promotes the visual cycle. Cell 154, 365–376.

Kirkegaard T, Roth AG, Petersen NH, Mahalka AK, Olsen OD, Moilanen I, Zylicz A, Knudsen J, Sandhoff K, Arenz C, *et al.* (2010). Hsp70 stabilizes lysosomes and reverts Niemann-Pick disease-associated lysosomal pathology. Nature 463, 549–553.

Klionsky DJ, Abdalla FC, Abeliovich H, Abraham RT, Acevedo-Arozena A, Adeli K, Agholme L, Agnello M, Agostinis P, Aguirre-Ghiso JA, *et al.* (2012). Guidelines for the use and interpretation of assays for monitoring autophagy. Autophagy 8, 445–544.

Ko DC, Gordon MD, Jin JY, Scott MP (2001). Dynamic movements of organelles containing Niemann-Pick C1 protein: NPC1 involvement in late endocytic events. Mol Biol Cell 12, 601–614.

Koga H, Kaushik S, Cuervo AM (2010). Altered lipid content inhibits autophagic vesicular fusion. FASEB J 24, 3052–3065.

Kornhuber J, Tripal P, Reichel M, Muhle C, Rhein C, Muehlbacher M, Groemer TW, Gulbins E (2010). Functional inhibitors of acid sphingomyelinase (FIASMAs): a novel pharmacological group of drugs with broad clinical applications. Cell Physiol Biochem 26, 9–20.

Kreitzer G, Schmoranzer J, Low SH, Li X, Gan Y, Weimbs T, Simon SM, Rodriguez-Boulan E (2003). Three-dimensional analysis of post-Golgi carrier exocytosis in epithelial cells. Nat Cell Biol 5, 126–136.

Kunchithapautham K, Rohrer B (2007a). Apoptosis and autophagy in photoreceptors exposed to oxidative stress. Autophagy 3, 433–441.

Kunchithapautham K, Rohrer B (2007b). Autophagy is one of the multiple mechanisms active in photoreceptor degeneration. Autophagy 3, 65–66.

Lakkaraju A, Finnemann SC, Rodriguez-Boulan E (2007). The lipofuscin fluorophore A2E perturbs cholesterol metabolism in retinal pigment epithelial cells. Proc Natl Acad Sci USA 104, 11026–11031.

Lebrand C, Corti M, Goodson H, Cosson P, Cavalli V, Mayran N, Faure J, Gruenberg J (2002). Late endosome motility depends on lipids via the small GTPase Rab7. EMBO J 21, 1289–1300.

Lee JK, Jin HK, Park MH, Kim BR, Lee PH, Nakauchi H, Carter JE, He X, Schuchman EH, Bae JS (2014). Acid sphingomyelinase modulates the autophagic process by controlling lysosomal biogenesis in Alzheimer's disease. J Exp Med 211, 1551–1570.

Le Guezennec X, Brichkina A, Huang YF, Kostromina E, Han W, Bulavin DV (2012). Wip1-dependent regulation of autophagy, obesity, and atherosclerosis. Cell Metab 16, 68–80.

Liu D, Meckel T, Long EO (2010). Distinct role of rab27a in granule movement at the plasma membrane and in the cytosol of NK cells. PLoS One 5, e12870.

Mackeh R, Perdiz D, Lorin S, Codogno P, Pous C (2013). Autophagy and microtubules—new story, old players. J Cell Sci 126, 1071–1080.

Nixon RA (2013). The role of autophagy in neurodegenerative disease. Nat Med 19, 983–997.

Pampliega O, Orhon I, Patel B, Sridhar S, Diaz-Carretero A, Beau I, Codogno P, Satir BH, Satir P, Cuervo AM (2013). Functional interaction between autophagy and ciliogenesis. Nature 502, 194–200.

Perdiz D, Mackeh R, Pous C, Baillet A (2011). The ins and outs of tubulin acetylation: more than just a post-translational modification? Cell Signal 23, 763–771.
Pikuleva IA, Curcio CA (2014). Cholesterol in the retina: the best is yet to come. Prog Retin Eye Res 41, 64–89.
Pipalia NH, Hao M, Mukherjee S, Maxfield FR (2007). Sterol, protein and lipid trafficking in Chinese hamster ovary cells with Niemann-Pick type C1 defect. Traffic 8, 130–141.
Polson HE, de Lartigue J, Rigden DJ, Reedijk M, Urbe S, Clague MJ, Tooze SA (2010). Mammalian Atg18 (WIPI2) localizes to omegasome-anchored phagophores and positively regulates LC3 lipidation. Autophagy 6, 506–522.
Radu RA, Hu J, Yuan Q, Welch DL, Makshanoff J, Lloyd M, McMullen S, Travis GH, Bok D (2011). Complement system dysregulation and inflammation in the retinal pigment epithelium of a mouse model for Stargardt macular degeneration. J Biol Chem 286, 18593–18601.
Reed NA, Cai D, Blasius TL, Jih GT, Meyhofer E, Gaertig J, Verhey KJ (2006). Microtubule acetylation promotes kinesin-1 binding and transport. Curr Biol 16, 2166–2172.
Reme CE, Wolfrum U, Imsand C, Hafezi F, Williams TP (1999). Photoreceptor autophagy: effects of light history on number and opsin content of degradative vacuoles. Invest Ophthalmol Vis Sci 40, 2398–2404.
Rocha N, Kuijl C, van der Kant R, Janssen L, Houben D, Janssen H, Zwart W, Neefjes J (2009). Cholesterol sensor ORP1L contacts the ER protein VAP to control Rab7-RILP-p150^{Glued} and late endosome positioning. J Cell Biol 185, 1209–1225.
Rodriguez-Boulan E, Kreitzer G, Musch A (2005). Organization of vesicular trafficking in epithelia. Nat Rev Mol Cell Biol 6, 233–247.
Rodriguez-Muela N, Koga H, Garcia-Ledo L, de la Villa P, de la Rosa EJ, Cuervo AM, Boya P (2013). Balance between autophagic pathways preserves retinal homeostasis. Aging Cell 12, 478–488.
Rubinsztein DC, Gestwicki JE, Murphy LO, Klionsky DJ (2007). Potential therapeutic applications of autophagy. Nat Rev Drug Discov 6, 304–312.
Sarkar S, Carroll B, Buganim Y, Maetzel D, Ng AH, Cassady JP, Cohen MA, Chakraborty S, Wang H (2013). Impaired autophagy in the lipid-storage disorder Niemann-Pick type C1 disease. Cell Rep 5, 1302–1315.
Sasaki T, Hazeki K, Hazeki O, Ui M, Katada T (1996). Focal adhesion kinase (p125FAK) and paxillin are substrates for sphingomyelinase-induced tyrosine phosphorylation in Swiss 3T3 fibroblasts. Biochem J 315, 1035–1040.
Sparrow JR, Gregory-Roberts E, Yamamoto K, Blonska A, Ghosh SK, Ueda K, Zhou J (2012). The bisretinoids of retinal pigment epithelium. Prog Retin Eye Res 31, 121–135.
Toops KA, Tan LX, Lakkaraju A (2014). A detailed three-step protocol for live imaging of intracellular traffic in polarized primary porcine RPE monolayers. Exp Eye Res 124, 74–85.
Travis GH, Golczak M, Moise AR, Palczewski K (2007). Diseases caused by defects in the visual cycle: retinoids as potential therapeutic agents. Annu Rev Pharmacol Toxicol 47, 469–512.
van Leeuwen R, Tomany SC, Wang JJ, Klein R, Mitchell P, Hofman A, Klein BE, Vingerling JR, Cumming RG, de Jong PT (2004). Is medication use associated with the incidence of early age-related maculopathy? Pooled findings from 3 continents. Ophthalmology 111, 1169–1175.
Wang L, Cano M, Handa JT (2014). p62 provides dual cytoprotection against oxidative stress in the retinal pigment epithelium. Biochim Biophys Acta 1843, 1248–1258.
Weng J, Mata NL, Azarian SM, Tzekov RT, Birch DG, Travis GH (1999). Insights into the function of Rim protein in photoreceptors and etiology of Stargardt's disease from the phenotype in *abcr* knockout mice. Cell 98, 13–23.
Xu J, Toops KA, Diaz F, Carvajal-Gonzalez JM, Gravotta D, Mazzoni F, Schreiner R, Rodriguez-Boulan E, Lakkaraju A (2012). Mechanism of polarized lysosome exocytosis in epithelial cells. J Cell Sci 125, 5937–5943.
Yao J, Jia L, Shelby SJ, Ganios AM, Feathers K, Thompson DA, Zacks DN (2014). Circadian and non-circadian modulation of autophagy in photoreceptors and retinal pigment epithelium. Invest Ophthalmol Vis Sci 55, 3237–3246.
Zhao C, Yasumura D, Li X, Matthes M, Lloyd M, Nielsen G, Ahern K, Snyder M, Bok D, Dunaief JL, *et al*. (2011). mTOR-mediated dedifferentiation of the retinal pigment epithelium initiates photoreceptor degeneration in mice. J Clin Invest 121, 369–383.